Fabrication and Quality Assessment of Thin Fins Built Using Metal Powder Bed Fusion Additive Manufacturing

Alexander J. Dunbar[1], Gabrielle J. Gunderman[1], Morgan C. Mader[2], and Edward W. Reutzel[1]

[1]Applied Research Lab, The Pennsylvania State University (CIMP-3D)

[2]Honeywell | Aerospace

Powder bed fusion additive manufacturing (PBFAM) is well suited for the fabrication of metallic components with thin features that would be otherwise impractical using other manufacturing methods. As component designs begin to take full advantage of the capabilities of additive manufacturing, so must the capability of measurement techniques used in assessment of quality increase. The characterization of quality may be application specific, requiring different metrics for different uses, e.g. impact on thermal vs. mechanical considerations. Here, thin fins are built with a wide range of processing conditions to test the limits of thin, metallic components using PBFAM. These thin fins are inspected using novel computed tomography (CT) based measurement techniques to assess their build quality. Within the process parameters tested, fins were successfully built thinner than manufacturer-recommended minimum wall thickness using default process parameters. The quality of these fins was assessed utilizing post-build non-destructive evaluation techniques developed herein.

Keywords: Powder bed fusion, CT, Inconel 625, Heat exchanger

Introduction

Powder bed fusion additive manufacturing (PBFAM) technology enables unique designs that revolutionize many of the traditional manufacturing design guidelines and principles. In particular, PBFAM provides the opportunity to design and fabricate structures with thin internal structures that would otherwise be impossible for more traditional subtractive manufacturing methods. Of particular interest is the use of PBFAM in the design and construction of heat exchangers, which benefit from light weighting and advanced geometries [1], [2].

Additive manufacturing is well suited for the manufacture of heat transfer components. Though for many applications the surface roughness present of as-built PBFAM components represents a hindrance in its application due to reduction in fatigue properties [3], for heat transfer applications, the increased surface roughness can be of benefit in enhancing convective heat transfer [4]–[6]. Potential improvements to heat exchangers with PBFAM technology are not limited to increased surface roughness, but also include the complex and thin geometries made viable through its use [5], [7], [8].

While PBFAM is well suited to the design and fabrication of thin geometries that would be found within a heat exchanger, thin geometries may result in further complications. While commercial PBFAM systems come with material specific processing parameters for the fabrication of components, previous studies have shown that these parameters may not be ubiquitous to all part geometries [9], [10]. Yadroitsev et al. (2007) demonstrated that effective processing parameters may also be dependent not only on material, but also local geometry [11]. Based on these studies it is imperative to define process parameters that are specific to not only machine and material, but geometry as well.

Prior studies have shown that PBFAM heat exchangers can exceed the heat transfer capabilities of traditionally manufactured ones [8], [12], [13]. Further advancements are possible through redesign of heat exchangers specifically for additive manufacturing [13]. As part of this effort it is necessary to identify PBFAM system capabilities and define processing parameters that will produce optimal heat

exchanger features. This study seeks to define the limits of a PBFAM system in producing the thinnest fins that would be suitable for use in a heat exchanger. Fins are measured using novel X-Ray computed tomography (CT) based measurement techniques developed herein; measurements are compared to traditional cross-sectioning measurements.

Methodology

Thin fins at a range of different fin angles were all constructed on an EOS M280 PBFAM machine using Inconel 625 with 40 µm layers. Fin geometries, shown in Figure 1, include a pedestal to isolate the fin geometry from the build plate and to allow wire EDM removal of the fins without damage. The top surface of the pedestal is angled so that the fin is always built perpendicular to the surface. The fin angles, defined as the angle at which the fin is built with respect to the (X-Y) build plane, are varied (45°, 67.5°, and 90°) to assess the impact of fin angle on quality. Fins are built using a scan path, with single- double and offset-scan trajectories, along the length of the fin using a range of laser powers and scan velocities. To achieve this the fins themselves are designed as a zero thickness 2D surface geometry, and ascribing user-specified scan parameters to each fin.

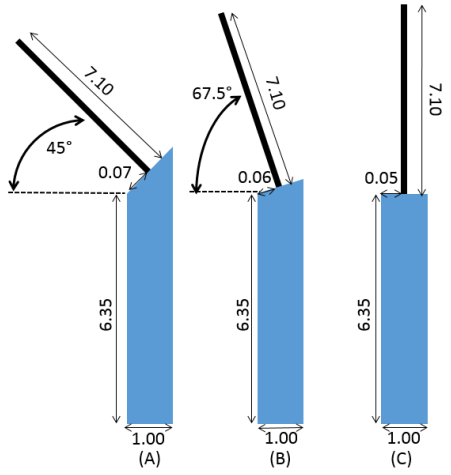

Figure 1: Schematic illustrating the fin and pedestal geometry and dimensions (in mm). All fins extend 9.65 mm into the page. (A) Fin angle 45° (B) Fin angle 67.5° (C) Fin angle 90°

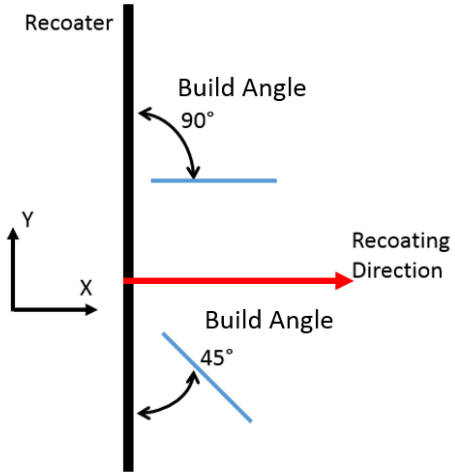

Figure 2: Schematic defining build angle for fins with the build direction perpendicular to the XY plane

Recognizing that recoater blade interference can also play a role in the quality of thin features, the build angle, defined as the angle between the fin and the recoater, as shown in Figure 2, was also varied. Only two build angles were used, where a build angle of 90° is defined as being perpendicular to the recoater and a build angle of 45° is defined as the fin being rotated 45° about the Z axis. Fins were spaced evenly with a constant radius about the center of the build plate, as shown in Figure 3 for the 45° build. A constant radius was used to reduce effects that may arise from variations in laser path length and angle-of-incidence. A summary of geometric parameters that are varied in this study can be found in Table 1.

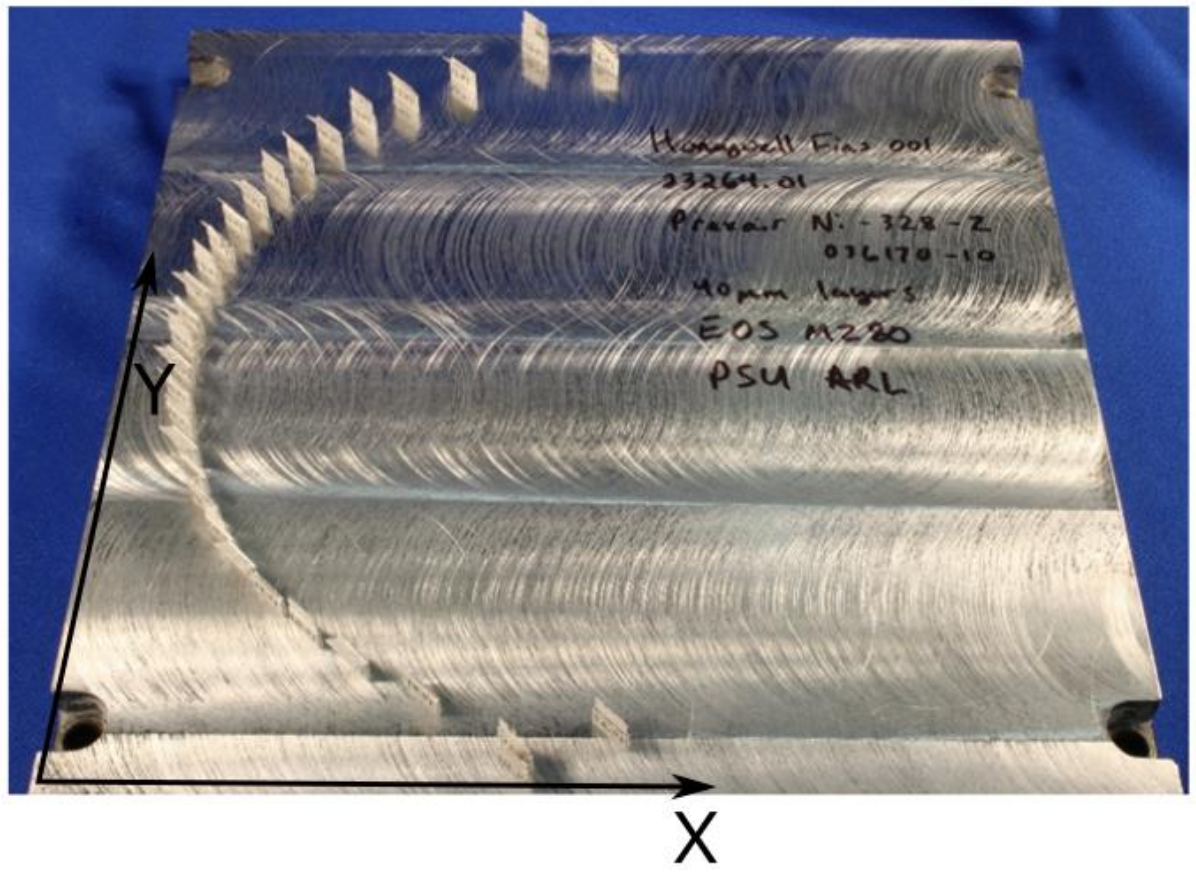

Figure 3: Build layout for fins built with 45° build angle

Table 1: Summary of geometric parameters varied in the fin study

Build Angle (°)	Fin Angle (°)
45	45
90	67.5
	90

Processing parameters altered within this study include: scan speed, laser power and the laser scan type. Power and scan speed are common parameters to vary in the definition of new process parameters [11]. The laser scan type determines the number of scan paths for each layer and the relative distances between the scan paths. For these fins, the laser scan type is used in place of the more common parameter, hatch spacing. Three different laser scan types are used: single, double, and offset. Fins built with the single laser scan type are built with only one laser path per layer. Fins built with the double laser scan type are built with two laser scan paths with each overlapped directly on one another. The final laser scan type, referred to as offset, is defined by two laser trajectories that are offset by 70 µm. The various process parameters used in the study are summarized in Table 2.

Table 2: Summary of process parameters used in fin study

Scan Speed (mm/s)	Laser Power (W)	Laser Scan Type
900	70	Single (S)
960	100	Double (D)
1500	285	Offset (O)

Due to the large number of processing and geometric parameters within this study, a complete design of experiment was not feasible. Instead, fin angle and laser scan type parameters were varied together to enable assessment across a larger parameter matrix. Table 3 shows a list of the parameter sets used for each build, i.e. one built with a 45° build angle, and the other built with a 90° build angle resulting in a full set of 56 test fins for the experiment.

Table 3: List of all fins built and their respective label and parameters.

Fin Name	Scan Speed (mm/s)	Power (W)	Fin Angle (°)	Laser Scan Type	Fin Name (Cont)	Scan Speed (mm/s)	Power (W)	Fin Angle (°)	Laser Scan Type
A#	900	70	90	S	N#	960	100	90	O
B#	900	70	67.5	D	O#	960	100	67.5	S
C#	900	70	45	O	P#	960	285	45	O
D#	900	100	90	D	Q#	960	285	90	S
E#	900	100	67.5	O	R#	960	285	67.5	D
F#	900	100	45	S	S#	1500	70	67.5	S
G#	900	285	90	O	T#	1500	70	45	D
H#	900	285	67.5	S	U#	1500	70	90	O
I#	900	285	45	D	V#	1500	100	67.5	D
J#	960	70	45	S	W#	1500	100	45	O
K#	960	70	90	D	X#	1500	100	90	S
L#	960	70	67.5	O	Y#	1500	285	67.5	O
M#	960	100	45	D	Z#	1500	285	45	S

In addition to the fins defined in Table 3, four fins were built using EOS M280 default processing conditions. Each of the default fins were designed to be a specified thickness: 300 µm, 200 µm, 100 µm, and 75 µm. Laser tool paths were defined automatically with fin geometries receiving the default laser scan path trajectories as defined by the EOS process software (PSW). These fins were built at two different build angles (45° and 90°) and only one fin angle (90°).

All fins from the study are subjected to 3D computed tomographic (CT) scanning using a GE phoenix v|tome|x system with a 300 kV microfocus tube. CT scan parameters were selected to provide 15 µm voxels for the fins. The CT scan data for each fin was processed using a thresholding technique to differentiate solid material. The threshold value was determined through a qualitative analysis. Fortunately, as the fins are very thin, scans have a high contrast between solid and void regions which provides a clear definition of both solid material. An example cross-section, comparing greyscale and binary images, for a fin is shown in Figure 4.

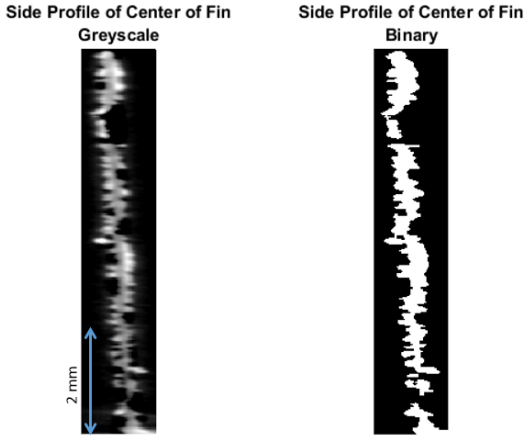

Figure 4: Comparison of greyscale (left) and binary (right) for a single fin slice.

Using the thresholded data, the median thickness and through-hole porosity of each fin were calculated within a user-defined central region of interest within each fin (to eliminate edge effects). The region of interest is 5mm wide and 2 mm tall and is centered on the fin. After CT scans were completed, each fin was also cross-sectioned, mounted, and polished in a destructive process for comparison. The thickness of each cross-sectioned fin was measured at five locations along the height. An example fin cross-sectioning measurement is shown in Figure 5 for fin H, which has a 67.5° fin angle and a 45° build angle. Although cross-sectional imaging is a more conventional measurement technique, when trying to assess the true thickness of the fin, it can be limiting. CT-based fin quality metrics allow for thickness and through-hole porosity measurements to be aggregated across a larger region of the fin area instead of confining measurements to individual cross-sectional areas.

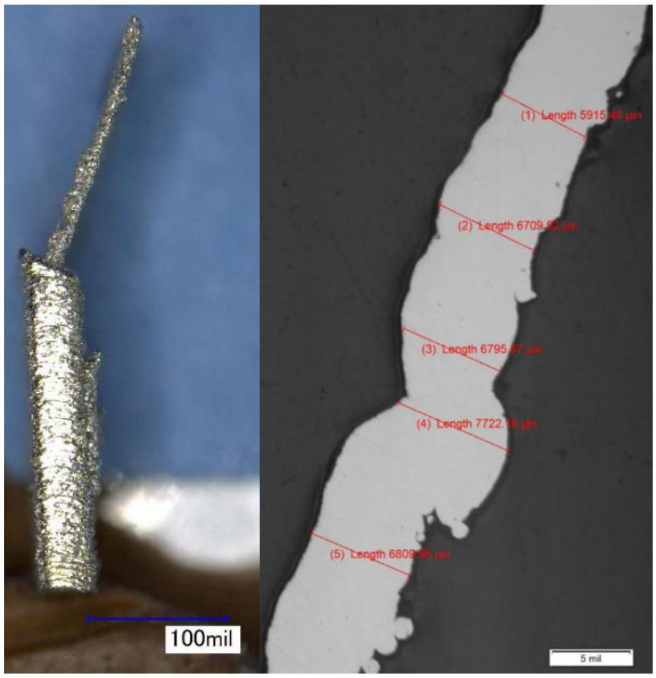

Figure 5: Fin H (Build angle 45°, Scan speed 900 mm/s, Power 285 W, Fin angle 67.5° and Laser scan type Single) as built image (left) and cross-sectional measurements (right) (Measurements in Imperial Units)

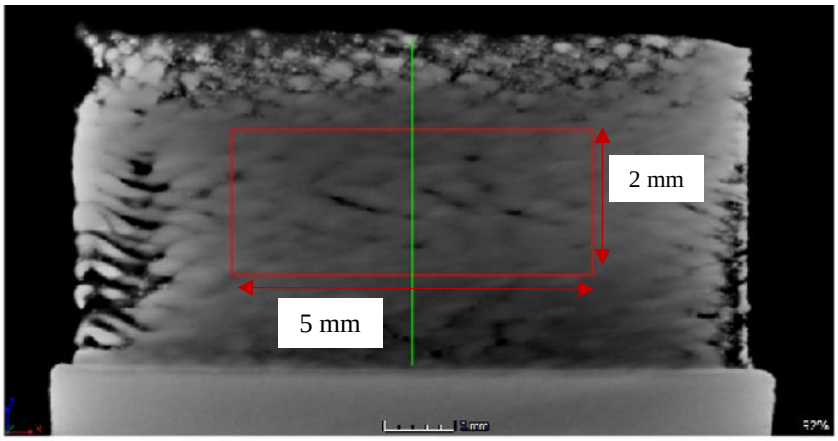

Figure 6: Single CT image of fin H with measurement regions highlighted. Region of interest (ROI) shown as a red rectangle and CT-based cross section region shown as a green line.

For thin AM components there is a great deal of variability in both through-hole porosity and thickness. For comparison, the CT-based measurements are taken for fin H across a single cross-section, defined by the green line in Figure 6, and a region of interest (ROI), defined by the red rectangle in Figure 6. CT-based cross sectioning and CT-based ROI measurements are compared against manual cross-sectioning measurements in Figure 7. Table 4 shows the comparisons of median thickness of the three different measurement techniques used. Between the three measurement techniques there is a significant discrepancy in the median thickness. Even between the two CT-based measurements, Figure 7-(B) and Figure 7-(C), there is a discrepancy of 30 µm in the median thickness. Figure 8, a contour map of fin thickness across the ROI, shows the variation in thickness across the region of interest. This discrepancy is not the result of measurement error, but instead a result of the complex surface in the relative

measurement region. The high variability of thickness across the fin defines the need for metrics that are aggregated across the surface of the fin to better asses the build quality.

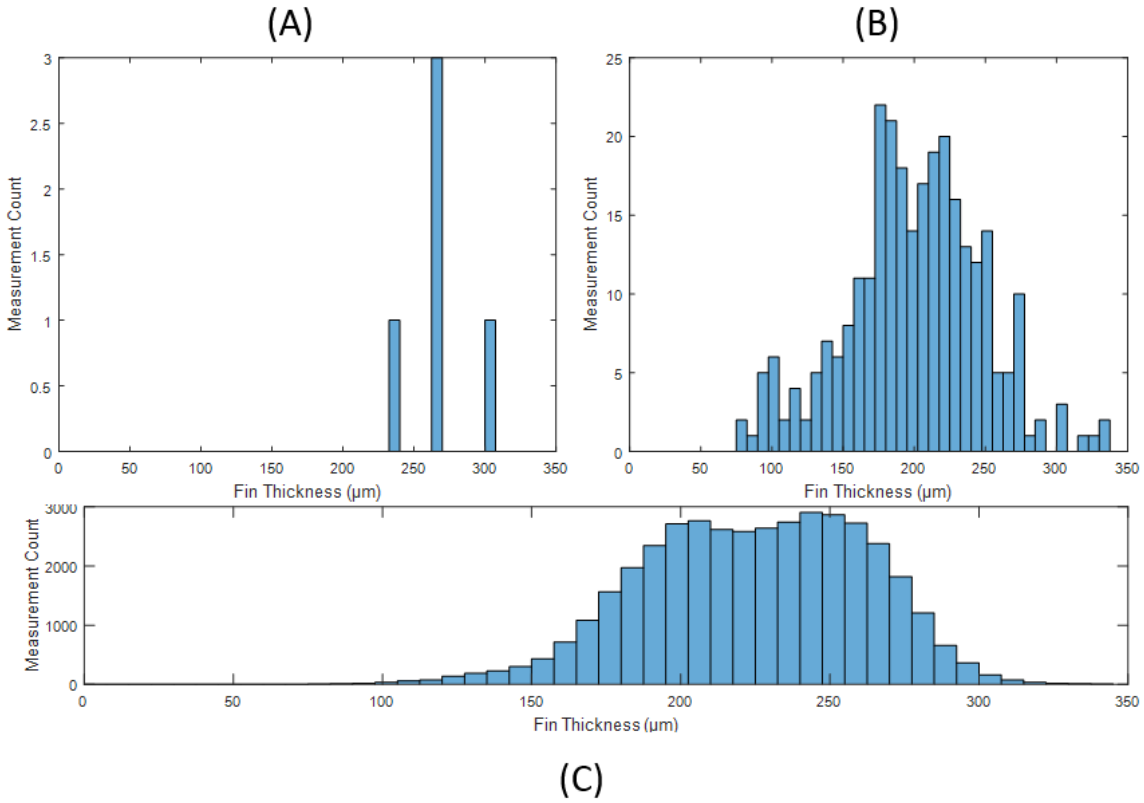

Figure 7: Histograms of measured fin thickness using different methods: (A) Manual Cross-Sectioning (Destructive) (B) CT-based measurement aggregated across a single cross-section (C) CT-based aggregated across an entire ROI.

Table 4: Comparison of measurement techniques for median thickness of a fin.

Measurement Technique	Number of Measurements Per Fin	Median Thickness (μm)
Physical Cross-Sectioning	5-6	267.5
CT Cross-Sectioning	~500	190
CT Region of Interest	~40,000	225

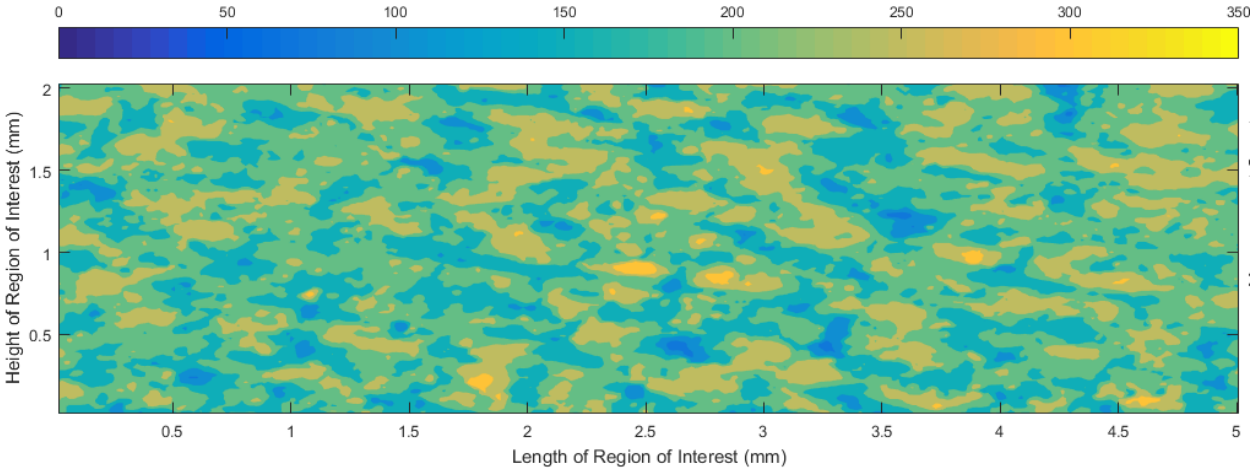

Figure 8: Contour map of thickness across the region of interest for fin H (as measured from CT scan data).

Results

A comparison of the median thickness measurements from the CT based analysis and the cross-sectioning measurement method is shown in Figure 9. The comparison between the manual cross-sectioning measurements and CT-based ROI measurements reveal that the CT-based measurements frequently exceed measurements from manual cross-sectioning. Although the percent difference in some of these cases exceeds 30% it is important to note that discrepancies can be due to both differences in measurement techniques as well as what is also likely due to differences in the region of the fin where the measurements are taken. The consistent agreement between the two methods provides adequate confidence in the CT-based ROI method, therefore all further analysis will be respective to CT measurements.

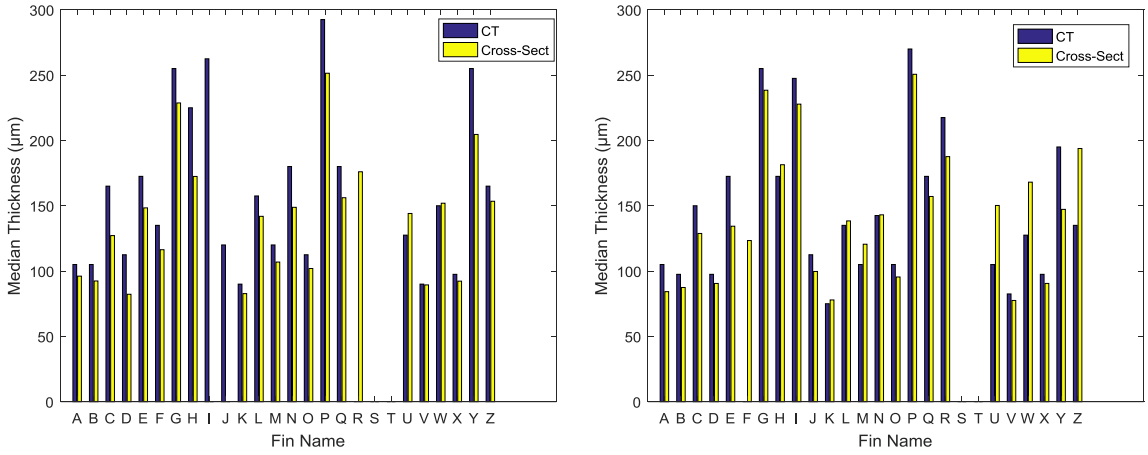

Figure 9: Comparison of median fin thickness from CT-based ROI measurement (CT) with manual cross-sectioning measurement (Cross-Sect) for build angle 45° (left) and 90° (right)

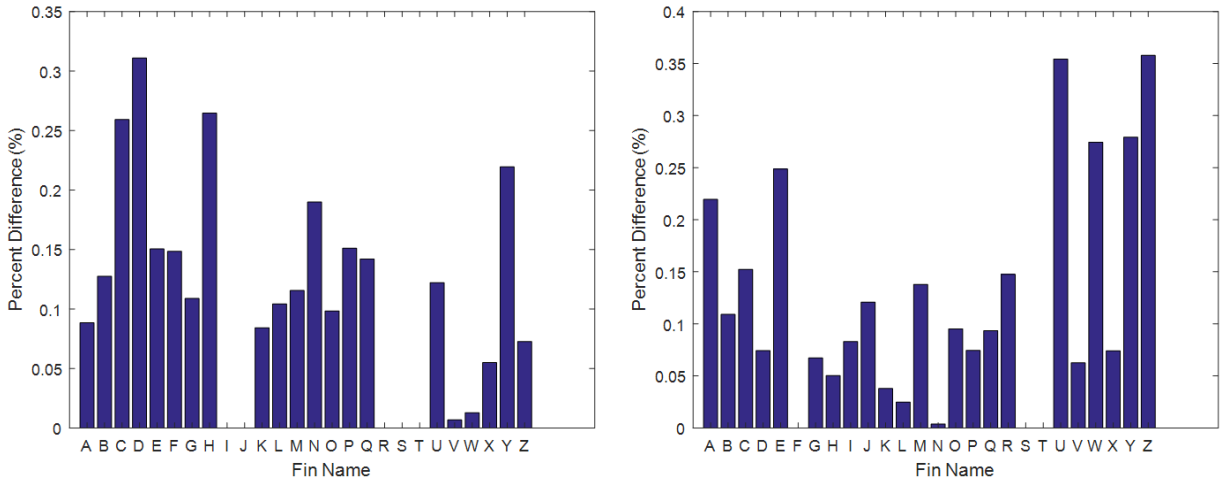

Figure 10:Percent difference in the median fin thickness between CT-based ROI measurements and manual cross-sectioning for build angle 45° (left) and 90° (right)

Figure 11 and Figure 12 show the median thickness and through-hole porosity, respectively, for all fins built within this study. Fins that failed to build are designated in Figure 12 as having 100% through-hole porosity. Fin thicknesses reported in Figure 11 demonstrate that for a given scan speed (V) there is an increase in fin thickness as laser power increases. Additionally, there is a second trend that shows that as the scan speed decreases the resultant fin thickness increases. Neither of these trends are surprising as an increase in laser power or decrease in scan speed result in more energy input to a given region. Increased energy deposited into a given volume will increase the melt pool size and therefore produce a thicker fin. Fins built with a build angle of 90° are consistently thicker than the matching fin built with a build angle of 45°. Figure 12, in conjunction with Figure 11, show that there is a trend where the thinner fins also exhibit the highest levels of through-hole porosity. The through-hole porosity and median thickness are also reported in Table 6.

The thinnest fins produced with no porosity were either scanned with a single or a double laser scan, since the overlap scan strategy consistently produced thicker fins. This is consistent with the initial supposition due to the increased area being scanned by the laser due to offset of 70 µm for that laser scan type. Sorting fins by highest through-hole porosity identifies that the single laser scan is most likely to exhibit a higher porosity, followed by the double laser scan, with the overlap laser scan having the lowest porosity. It should be noted that the single, double, and overlap laser scan types were not isolated parameters in the test plan defined in Table 3.

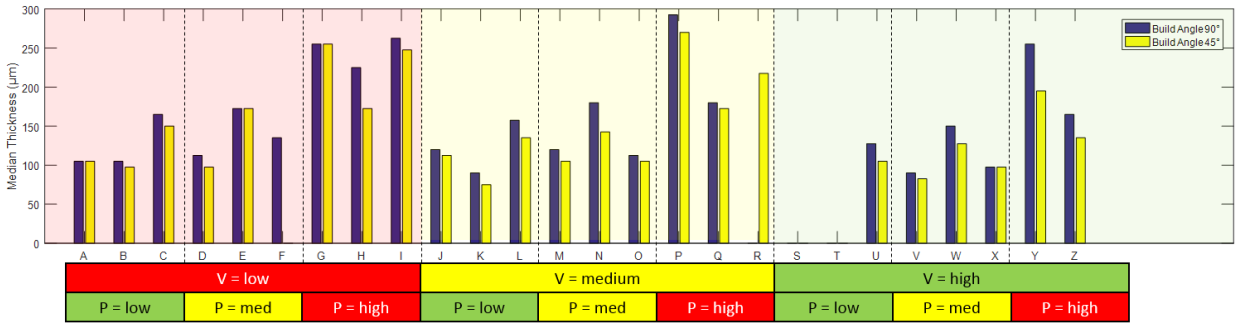

Figure 11: Median fin thickness for all fins built highlighting the laser power (P) and scan speed (V) parameters for each fin. For the values corresponding to high medium and low see Table 3.

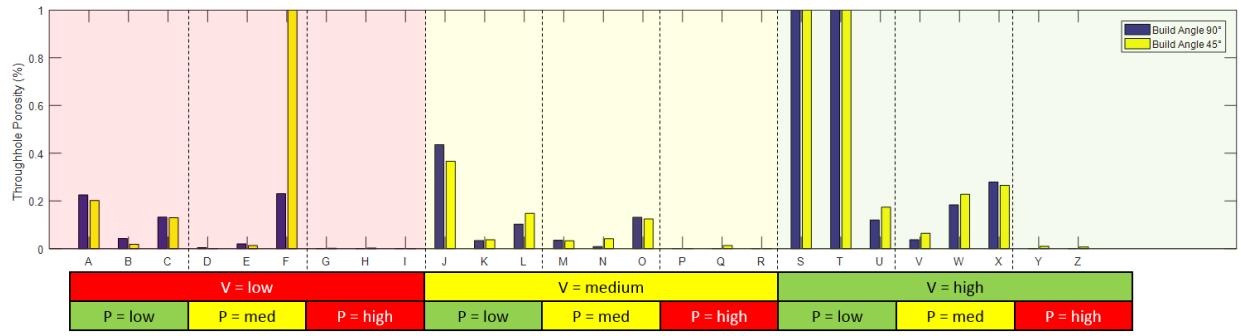

Figure 12: Percent through-hole porosity for all fins built highlighting the laser power (P) and scan speed (V) parameters for each fin. For the values corresponding to high medium and low see Table 3.

Figure 13 shows the median thickness and through-hole porosity of the fins built with the default EOS processing parameters and prescribed fin thickness defined in the Methodology section. In Figure 13 there is a discrepancy between the prescribed fin thickness and the measured thickness. For the fins with 300 µm prescribed thickness, the measured thickness is approximately 300 µm, but the fins designed with 200 µm, 100 µm and 75 µm wall thickness exhibit similar thicknesses and through-hole porosity. This is likely an effect of the scan strategy, where only the 300 µm thick fin has a hatching region and the discrepancy between the other fins is defined by the offset of the contours tracing the outline of the fin as defined by the EOS process software. Typical hatch spacing for a PBF machine is between 100 µm and 200 µm, which here would allow for hatches in the 300 µm fins.

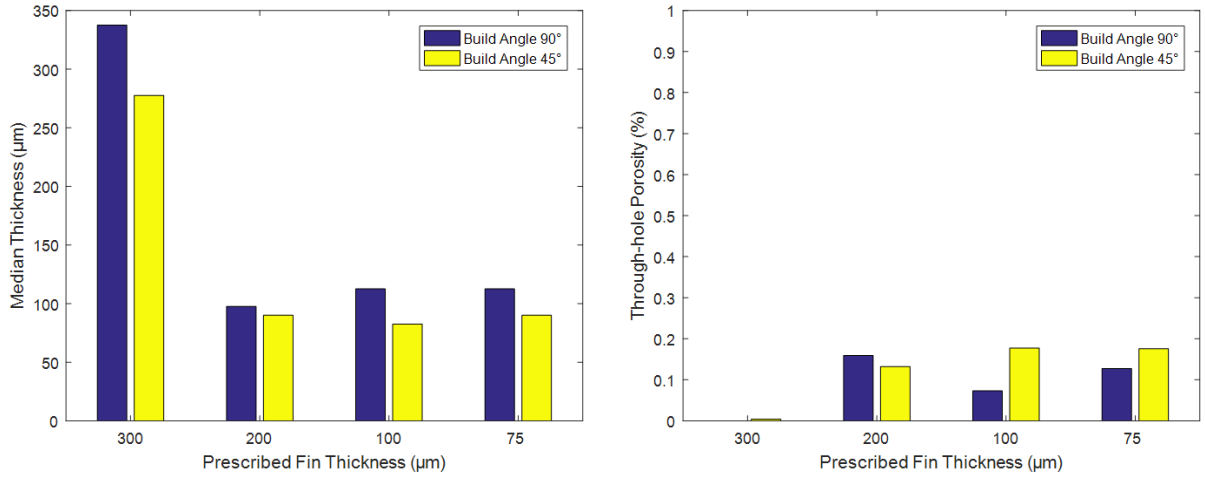

Figure 13: Median thickness and through-hole porosity of fins built with default EOS processing parameters and prescribed thickness

Discussion

For fins within the channel section of a heat exchanger (i.e. with the same fluid on either side of the fin), some porosity is acceptable as flow across the fin surface would not result in unwanted mixing. However, for a tube sheet, which separates two different fluids, the geometry must be capable of preventing mixing and sustaining a pressure differential between the two flows; which requires that no porosity is present. In this analysis, we have addressed this by defining two categories of fins: the thinnest fins with less than 10% porosity, and the thinnest fins with no porosity. Figure 14 highlights fins that match these definitions of successful fins.

Figure 14 shows median fin thickness for all fins that are built with no through-hole porosity (left) and meet the 10% through-hole porosity threshold (right). For the fins built with the parameters defined in Table 3, the thinnest fin with no porosity has a median thickness of 97.5 µm and the thinnest fin within the 10% porosity threshold has a median thickness of 75 µm. For the best fins there is also a strong agreement, within 10% difference, between the cross-sectioning measurements and the CT-based ROI measurements. For fins built with default EOS parameters, Figure 13, the only fins built with no porosity has a median thickness of 338 µm. The thinnest fin that meets the 10% porosity threshold has a median thickness of 113 µm. These best fins for the experimental and the standard EOS parameter set are listed in Table 5 for easy comparison.

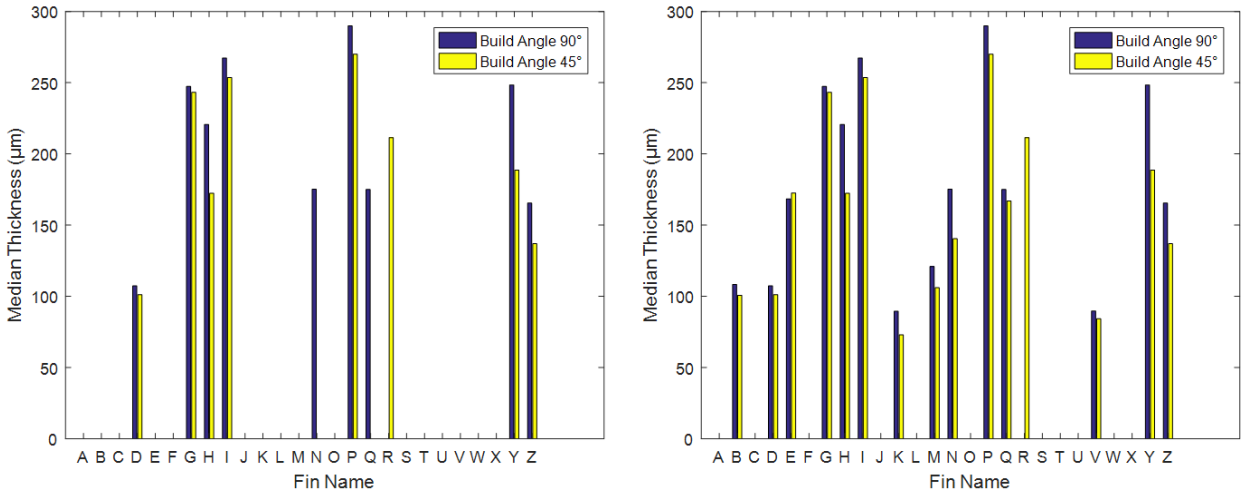

Figure 14: Median fin thickness of fins built with no through-hole porosity (left) and less than 10% through-hole porosity (right)

Table 5: Summary of the best fins built using the standard EOS parameters and experimental parameters from Table 3.

Fin Category	Standard EOS Parameter	Best with Parameter Development
Thinnest Fin with <10% porosity	113 µm (100 µm design / 90° build angle)	75 µm (Fin K / build angle 45°)
Thinnest Fin with no porosity	338 µm (300 µm design /90° build angle)	97.5 µm (Fin D /build angle 45°)

Conclusion

As part of this study, numerous fins were constructed using a range of process and geometric parameters. Within the parameter space tested, the fin thickness increases with either an increase in laser power or a decrease of scan speed. Fins were analyzed with a combination of CT-based measurements aggregated over a region of interest, developed herein, as well as physical measurements performed using destructive cross-sectioning. The CT-based measurement technique represents an advancement in inspection methods allowing geometric measurements to be made automatically, allowing for a larger and more representative region of interest to be used to quantify build quality.

Fins that were built with the parameters defined in Table 3 were compared against fins built with default EOS processing conditions. The best fins built with the varied processing conditions were thinner and less porous than the fins built with the default EOS processing conditions. Further development includes using the identified ideal processing parameters for fins in actual heat exchangers to test their effectiveness in working components. Future work also includes the development of additional measurement algorithms to determine other pertinent metrics to define fin quality using CT-based measurement techniques.

Acknowledgements

The authors gratefully acknowledge the contributions of Griffin Jones and Corey J. Dickman. This material is based on research sponsored by Air Force Research Laboratory under agreement number

FA8650-12-2-7230. The U.S. Government is authorized to reproduce and distribute reprints for Governmental purposes notwithstanding any copyright notation thereon.
Any opinions, findings and conclusions or recommendations expressed in this material are those of the authors and do not necessarily reflect the views of the Air Force Research Laboratory or the U.S. Government.

References

[1] R. Neugebauer, B. Müller, M. Gebauer, and T. Töppel, "Additive manufacturing boosts efficiency of heat transfer components," *Assem. Autom.*, vol. 31, no. 4, pp. 344–347, 2011.
[2] S. Zhang and W. Seiya, *3D Printing as an Alternative ManufacturingMethod for the Micro gas Turbine Heat Exchanger*. 2015.
[3] T. M. Mower and M. J. Long, "Mechanical behavior of additive manufactured, powder-bed laser-fused materials," *Mater. Sci. Eng. A*, vol. 651, pp. 198–213, Jan. 2016.
[4] T. P. Brackbill and S. G. Kandlikar, "Effects of low uniform relative roughness on single-phase friction factors in microchannels and minichannels," in *Proceedings of the International Conference on Nanochannels, Microchannels, and Minichannels. ICNMM2007-30031*, 2007, p. 97.
[5] M. Wong, I. Owen, C. J. Sutcliffe, and A. Puri, "Convective heat transfer and pressure losses across novel heat sinks fabricated by Selective Laser Melting," *Int. J. Heat Mass Transf.*, vol. 52, no. 1–2, pp. 281–288, Jan. 2009.
[6] W. Reed, M. von Spakovsky, and P. Raj, "Comparison of Heat Exchanger and Thermal Energy Storage Designs for Aircraft Thermal Management Systems," 2016.
[7] B. Brown, B. Brown, W. Everhart, W. Everhart, J. Dinardo, and J. Dinardo, "Characterization of bulk to thin wall mechanical response transition in powder bed AM," *Rapid Prototyp. J.*, vol. 22, no. 5, pp. 801–809, 2016.
[8] R. A. Felber, N. Rudolph, and G. F. Nellis, "Design and simulation of 3D printed air-cooled heat exchangers," in *Proceedings of Solid Freeform Fabrication Symposium*, 2016.
[9] M. Simonelli *et al.*, "A Study on the Laser Spatter and the Oxidation Reactions During Selective Laser Melting of 316L Stainless Steel, Al-Si10-Mg, and Ti-6Al-4V," *Metall. Mater. Trans. A*, vol. 46, no. 9, pp. 3842–3851, Sep. 2015.
[10] I. Yadroitsev, L. Thivillon, P. Bertrand, and I. Smurov, "Strategy of manufacturing components with designed internal structure by selective laser melting of metallic powder," *Appl. Surf. Sci.*, vol. 254, no. 4, pp. 980–983, Dec. 2007.
[11] I. Yadroitsev, P. Bertrand, and I. Smurov, "Parametric analysis of the selective laser melting process," *Appl. Surf. Sci.*, vol. 253, no. 19, pp. 8064–8069, Jul. 2007.
[12] J. C. Snyder, C. K. Stimpson, K. A. Thole, and D. Mongillo, "Build direction effects on additively manufactured channels," *J. Turbomach.*, vol. 138, no. 5, p. 051006, 2016.
[13] K. L. Kirsch and K. A. Thole, "Heat transfer and pressure loss measurements in additively manufactured wavy microchannels," *J. Turbomach.*, vol. 139, no. 1, p. 011007, 2017.

Appendix

Table 6: Median thickness and through-hole porosity of fins built with processing parameters defined in Table 3

Fin Name	Median Thickness 45° (µm)	Median Thickness 90° (µm)	Through-hole Porosity 45° (%)	Through-hole Porosity 90° (%)	Fin Name (Cont)	Median Thickness 45° (µm)	Median Thickness 90° (µm)	Through-hole Porosity 45° (%)	Through-hole Porosity 90° (%)
A#	103	101	0.225	0.202	N#	103	101	0.225	0.202
B#	108	101	0.042	0.018	O#	108	101	0.042	0.018
C#	155	142	0.132	0.129	P#	155	142	0.132	0.129
D#	107	101	0.004	0.000	Q#	107	101	0.004	0.000
E#	168	173	0.020	0.012	R#	168	173	0.020	0.012
F#	130	NA	0.230	NA	S#	130	NA	0.230	NA
G#	247	243	0.000	0.001	T#	247	243	0.000	0.001
H#	255	172	0.000	0.002	U#	255	172	0.000	0.002
I#	267	254	0.000	0.000	V#	267	254	0.000	0.000
J#	119	106	0.435	0.366	W#	119	106	0.435	0.366
K#	89	73	0.033	0.037	X#	89	73	0.033	0.037
L#	144	125	0.103	0.148	Y#	144	125	0.103	0.148
M#	121	106	0.035	0.033	Z#	121	106	0.035	0.033

Table 7: Median thickness and through-hole porosity of fins built with default EOS processing parameters and prescribed thickness

Defined Fin Thickness (µm)	Median Thickness 45° (µm)	Median Thickness 90° (µm)	Through-hole Porosity 45° (%)	Through-hole Porosity 90° (%)
300	338	278	0.000	0.004
200	98	90	0.159	0.132
100	113	83	0.073	0.177
75	113	90	0.127	0.176